Engineering Structures 238 (2021) 112179

Contents lists available at ScienceDirect

Engineering Structures

journal homepage: www.elsevier.com/locate/engstruct

# Numerical modeling approach for uhpfrc members including crack spacing formulations

Renaud Franssen [a,b,*], Serhan Guner [c], Luc Courard [b], Boyan I. Mihaylov [b]

[a] FRIA (F.R.S.-F.N.R.S), National Fund for Scientific Research, Brussels, Belgium
[b] ArGEnCo Department, Research Unit in Urban and Environmental Engineering, University of Liège, Allée de la Découverte 9, Liège 4000, Belgium
[c] Department of Civil Engineering, University of Toledo, 2801 W Bancroft St., MS 307, NI 3021, Toledo, OH 43606-3390, USA

ARTICLE INFO

*Keywords:*
UHPFRC beams
Finite element
Crack spacing
Flexural failure
Shear failure
Strain-hardening
Strain-softening

ABSTRACT

Ultra-high performance fiber-reinforced concrete (UHPFRC) possesses excellent mechanical properties and durability. The steel fibers in the concrete result in significant post-cracking tensile resistance and enhanced crack control. However, while UHPFRC is a promising material for the construction of new (and repair of existing) infrastructure, its application is still limited—in part due to the lack of numerical models with the capacity to simulate its complex behavior. To help overcome this challenge, this study proposes a numerical material modeling approach for the nonlinear finite element analysis of UHPFRC. The approach aims to provide a general applicability to model both shear- and flexure-critical members made from strain-softening or -hardening UHPFRC, while still using simple equations. This objective can be achieved by establishing a comprehensive set of crack spacing formulations and modeling recommendations to capture the unique behavior of UHPFRC. The crack spacing estimates are used together with the Diverse Embedment Model for FRC, which is extended here for the modeling of UHPFRC. When applied to 29 flexure- and shear-critical specimens, the proposed modeling approach accurately simulates the experimental responses with an average of 1.04 and a coefficient of variation of 10.2% for the experimental-to-predicted strength ratios.

## 1. Introduction

Ultra-high performance fiber-reinforced concrete (UHPFRC) has emerged as a new class of material that offers excellent mechanical properties [1,2]. As compared to regular concrete, UHPFRC is about five to six times stronger in both compression and tension, with compressive and tensile strengths of up to 250 and 12 MPa, respectively. Due to the presence of steel fibers in the cement matrix, UHPFRC possesses significant post-cracking tensile resistance, and can be designed to exhibit ductile strain-hardening behavior in tension. This behavior provides a highly effective crack control which, together with the low porosity of the cement matrix, results in excellent durability in aggressive environments [3–5]. UHPFRC also enables the use of smaller section sizes, resulting in lighter structures with the potential benefits of smaller seismic forces and more economical foundations. These properties make UHPFRC an ideal candidate for not only the construction of next-generation infrastructure, but also the rehabilitation and strengthening of existing infrastructure.

While design guidelines and code provisions are continuously being developed for UHPFRC in France [6], Switzerland [7], Japan [8], and Australia [9], a number of obstacles hinder the widespread application of this material. One of them is the complex behavior of UHPFRC members (involving concrete, fibers, reinforcing bars, and the bond in between them); another is the lack of fully developed and validated numerical models to simulate these behaviors. Most current studies on numerical modeling include the use of commercial finite element software, which is not specialized for UHPFRC [10–12], while others propose theoretical formulations that require complex implementations in computer codes [13,14]. As most existing models are based on the smeared crack approach, an important remaining problem is the evaluation of the crack spacing in flexure- and shear-critical members, which affects the predicted ductility of the UHPFRC, and therefore the predicted response of the member. Furthermore, special, experimentally-determined material properties—required as input to numerical models—create an additional challenge.

To help overcome the current challenges, this study proposes a numerical material modeling approach for the nonlinear finite element analysis of UHPFRC. The proposed approach extends the Simplified

* Corresponding author at: FRIA (F.R.S.-F.N.R.S), National Fund for Scientific Research, Brussels, Belgium.
*E-mail address:* r.franssen@uliege.be (R. Franssen).

https://doi.org/10.1016/j.engstruct.2021.112179
Received 25 June 2020; Received in revised form 17 February 2021; Accepted 2 March 2021
Available online 5 April 2021

**Table 1**
Input properties for UHPFRC.

| Material property | Input values |
|---|---|
| Compressive strength $f_c'$ | From experiment |
| Tensile strength $f_{ct}$ | From experiment or $0.6\sqrt{f_c'}$ [17] |
| Initial tangent modulus $E_c$ | From experiment or $50GPa$ [6] |
| Fiber bond strength | $0.75\sqrt{f_c'}$ |

Diverse Embedment Model (SDEM) [15], which was originally developed for fiber reinforced concrete, to model UHPFRC. The main objective of the proposed approach is to provide a general applicability to model both shear- and flexure-critical members made from strain-softening or -hardening UHPFRC materials, while using simple equations and basic material property inputs. To account for the location of the main flexural reinforcing bars and the presence (or absence) of shear reinforcement, a set of crack spacing formulations are established. In addition, a new bond resistance limit is proposed to account for the high density and high cement content of the UHPFRC. The proposed approach is validated with 29 large-scale beam specimens tested by seven different research groups. The specimens include 14 shear-critical (eight with no shear reinforcement) and 15 flexural-critical members, with 11 flanged and 18 rectangular sections. The simulated load, deflection, cracking, and failure behaviors are examined in detail and compared with the experimentally measured data. The following sections discuss the formulation, application, and validation of this modeling approach.

## 2. Formulation

### 2.1. Extension of the simplified diverse embedment model for UHPFRC

The Diverse Embedment Model (DEM) [16] was originally developed for normal strength fiber reinforced concrete (FRC). It is based on modeling the behavior of a single straight or hooked fiber across a crack in the concrete, where the fiber is unsymmetrically embedded on both sides of the crack. The deformations of the fiber are neglected and the bond-slip behavior of the interface with the surrounding concrete is assumed elastic-perfectly-plastic. The maximum bond resistance for straight fibers is estimated at $0.369\sqrt{f_c'}$ (MPa), where $f_c'$ is the compressive strength of the FRC. This model results in the following expressions for the average fiber stress $\sigma_{f,cr,avg}$ and normal stress per unit crack area $\sigma_f$:

$$\sigma_{f,cr,avg} = \frac{2}{l_f}\int_0^{l_f/2}\int_0^{\pi/2}\sigma_{f,cr}(w,l_a,\theta)\sin\theta d\theta dl_a \quad (1)$$

$$\sigma_f = \alpha_f V_f \sigma_{f,cr,avg} \quad (2)$$

where $\sigma_{f,cr}$ is the stress in a single fiber; $w$ is the crack width; $l_f$ is the fiber length; $l_a$ is the shorter embedment length of the fiber; $\theta$ is the angle of the fiber with respect to the direction normal to the crack; $\alpha_f$ is a fiber orientation factor; and $V_f$ is the volumetric ratio of fibers. To increase the computational efficiency of the DEM for finite element simulations, Lee et al. [15]. simplified Eqs. (1) and (2) to close-form equations and proposed the Simplified Diverse Embedment Model (SDEM).

The behavior of fibers across cracks in UHPFRC is similar to that described by the DEM (or SDEM). The fibers in UHPFRC are typically straight and are pulled out of the cement matrix as the crack opens. Consequently, the SDEM presents a potential for modeling UHPFRC. Modeling of tests performed in this study demonstrated that the maximum bond resistance $\tau_{fm}$ used in the SDEM is too low for adequately accounting for the high density and high cement content of the UHPFRC matrix. Using the test data available in the literature, a new relationship is conceived for the proposed modeling approach as $\tau_{fm} = 0.75\sqrt{f_c'}$ (MPa), where $f_c'$ is the compressive strength of the UHPFRC. In addition, the material property values shown in Table 1 are found suitable for UHPFRC and are used in the proposed modeling approach.

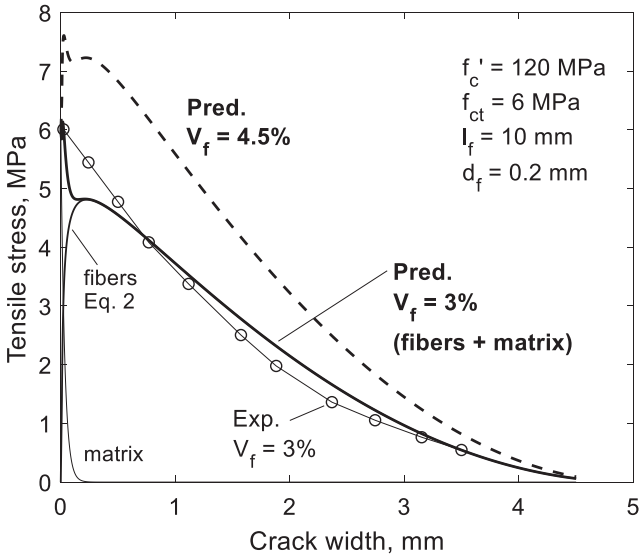


**Fig. 1.** Measured and predicted tension response of UHPFRC – test by Garneau [18].

Fig. 1 shows a sample comparison performed for an UHPFRC mix with $f_c' = 120$ MPa, $f_{ct} = 6.0$ MPa, $V_f = 3.0\%$, $l_f = 10$ mm, and $d_f = 0.2$ mm [18]—where $f_{ct}$ is the tensile strength (i.e., cracking stress) of the matrix. The material was tested in pure tension and developed a single crack as characteristic of a softening UHPFRC. The figure shows that the SDEM captures the decrease in the tensile resistance as a function of the crack opening all the way to the complete pull-out of the fibers off the matrix. The SDEM prediction consists of two contributions: the contribution of the fibers described by Eq. (2), and the tension-softening behavior of the cement matrix across the crack, labeled "matrix".

In addition to the behavior of softening UHPFRC, Fig. 1 also shows a comparison between the predicted softening and hardening behaviors. The two SDEM curves in the plot are generated for the same UHPFRC material, except that the fiber volume ratio is increased from 3% to 4.5%. The figure shows that a $V_f$ ratio of 4.5% produces a hardening behavior, where the peak tensile resistance exceeds the cracking strength $f_{ct} = 6$ MPa. This behavior is characterized by the formation of multiple cracks, instead of a single crack that leads to the failure of softening UHPFRC.

### 2.2. Tension behavior of reinforced UHPFRC members

After adapting the SDEM to model UHPFRC, the next step is to model the tension behavior of UHPFRC members with reinforcing bars (i.e., reinforced UHPFRC). The combination of fibers and rebars results in the formation of closely spaced cracks and more uniform deformations. Consequently, the proposed modeling framework employs the smeared crack approach, as formulated by Lee et al. [19] for FRC. In this approach, the constitutive relationships of concrete, fibers, and rebars are expressed in terms of average stresses as functions of the average strain measured across several cracks $\varepsilon_c$.

Using average stresses, the axial force in a tension member with a cross-sectional area $A_c$ is expressed as:

$$N = \left[\rho_s\sigma_s + \alpha_{avg}\sigma_f + \sigma_{c,TS} + (1-\alpha_{avg})\sigma_f\right]A_c = N_s + N_f + N_{c,TS} + N_{c,f} \le \left(\rho_s f_y + \sigma_f\right)A_c \quad (3)$$

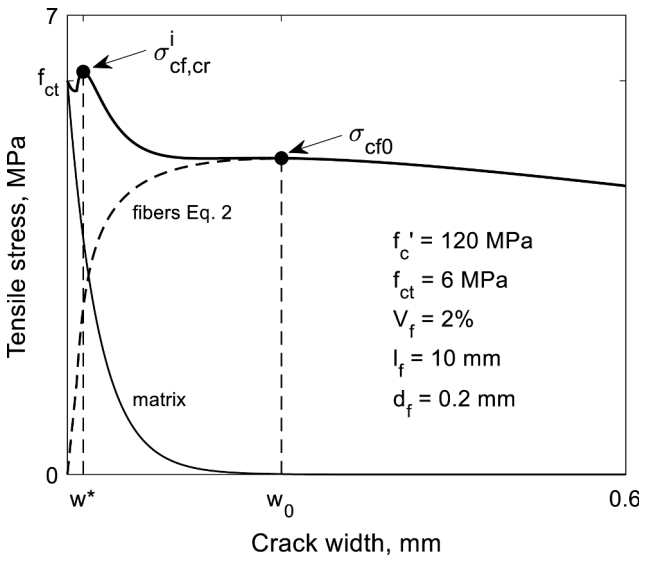


**Fig. 2.** Important stress and crack width values from the tension response of UHPFRC.

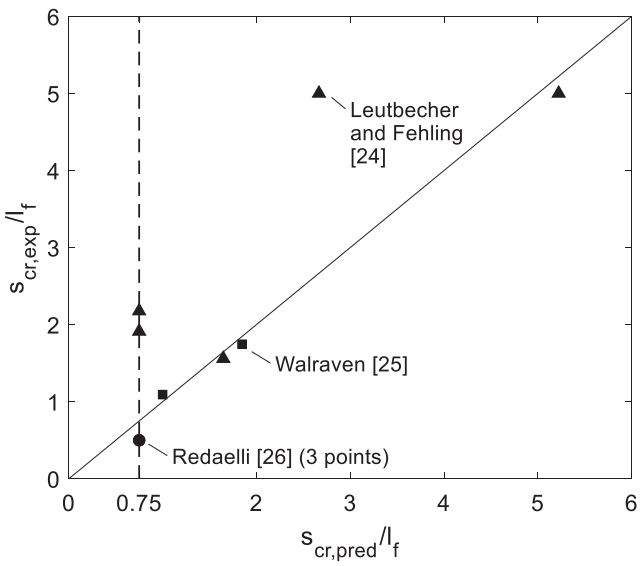


**Fig. 3.** Measured vs. predicted average crack spacing for 10 reinforced UHPFRC members subjected to uniaxial tension.

where $\rho_s$ is the reinforcement ratio; $\sigma_s$ is the average stress in the rebars; $\sigma_f$ is the stress in the fibers in the crack; $\alpha_{avg}\sigma_f$ is the average stress in the fibers; $f_{c,TS}$ is the average stress in the concrete due to the bond with the rebars (i.e., tension stiffening effect); and $(1\text{-}\alpha_{avg})\sigma_f$ is the average stress in the concrete due to the bond with the fibers. The stress-strain relationship of the steel $\sigma_s(\varepsilon_c)$ is assumed elastic-perfectly-plastic; $f_{c,TS}(\varepsilon_c)$ is evaluated as proposed by Lee et al. [19]; and $\sigma_f$ is evaluated from the SDEM. However, as the SDEM is based on the width of the crack $w$, while the smeared crack approach is based on the average strain $\varepsilon_c$, it is necessary to express $w$ with $\varepsilon_c$ as follows:

$$w = \varepsilon_c k_w s_{cr}$$
$$k_w = 1.7 + 3.4\frac{V_f l_f}{d_f} \tag{4}$$

where $s_{cr}$ is the basic crack spacing and factor $k_w$ was proposed by Deluce et al. [20] to capture the width of the widest crack that governs the ultimate response of tension members. Consequently, a crucial aspect in the numerical modeling of UHPFRC structures is the evaluation of $s_{cr}$. As compared to reinforced concrete members, the addition of fibers results in more closely spaced cracks.

To evaluate $s_{cr}$ in the vicinity of the rebars, the following expression is adopted based on the work of Leutbecher and Fehling [21,22]:

$$s_{cr} = \frac{\left(\sigma^{i}_{cf,cr} - \sigma_{cf0}\right)d_s}{2\tau_{sm}\rho_s} \geq 0.75 l_f \tag{5}$$

where $\sigma^{i}_{cf,cr}$ is an imaginary cracking stress of the UHPFRC that takes into account the effect of the fibers at very small crack widths; $\sigma_{cf0}$ is the maximum tensile stress that the fibers can transfer across a crack; $d_s$ is the diameter of the rebars; $\tau_{sm}$ is the average bond stress over the load-transmission length between the bar and matrix $\approx 2.5\tau_{fm}$ [17] (i.e. $\tau_{sm} \approx 1.90\sqrt{f_c'}$ MPa); $\rho_s$ is the ratio of steel reinforcement; and $l_f$ is the fiber length. The left-hand-side of Eq. (5) was derived by considering the equilibrium of a concrete region bound by a crack and the nearest section where a new crack can form. It represents the maximum crack spacing within the assumptions made in the derivation, while additional unfavorable effects such as the scatter in material properties and non-uniform stress distributions are approximately accounted for with the empirical factor $k_w$ in Eq. (4). The lower bound on the crack spacing imposed in Eq. (5) takes into account the length over which the fibers transfer tension to the concrete on each side of a crack [23]. This limit governs in reinforced UHPFRC members with large amounts of reinforcement and/or fibers. The cracks spacing of $0.75l_f$ is also used for UHPFRC without reinforcement that exhibits strain-hardening behavior. It should be noted that the combination of factor $k_w$ and Eq. (5) adopted here is meant to produce somewhat conservative crack width estimates.

Stresses $\sigma^{i}_{cf,cr}$ and $\sigma_{cf0}$ are illustrated in Fig. 2, which is an enlarged version of Fig. 1. The imaginary cracking stress develops at a crack width $w^*$ when the matrix is in the tension softening regime and the fibers are in the activation regime:

$$\sigma^{i}_{cf,cr} = f_{ct}\left(1 - w^*\cdot\frac{f_{ct}}{2G_F}\right) + \sigma_{cf0}\left(2\sqrt{\frac{w^*}{w_0}} - \frac{w^*}{w_0}\right) \tag{6}$$

$$w^* = w_0\left(1 + \frac{w_0 f_{ct}^2}{2\sigma_{cf0}G_F}\right)^2 \tag{7}$$

where $G_F$ is the fracture energy of the matrix [17] estimated at 0.06 N/mm. The cracking stress of the matrix $f_{ct}$ is obtained from material testing or, if test results are not available, it can be estimated at $0.60\sqrt{f_c'}$ (MPa)—derived based on comparisons with material tests from the literature. Finally, stress $\sigma_{cf0}$ and corresponding crack width $w_0$ are determined from [17]:

$$\sigma_{cf0} = \alpha_f V_f \frac{\tau_{fm} l_f}{d_f} \tag{8}$$

$$w_0 = \frac{\tau_{fm} l_f^2}{E_f d_f} \tag{9}$$

where $E_f \approx 200$ GPa is the modulus of elasticity of the fibers.

To validate the above equations, 10 tension tests of prismatic reinforced UHPFRC members were collected from the literature [21,24–26]. In Fig. 3, the experimentally obtained crack spacing is plotted versus the predictions of Eq. (5)—both normalized with respect to the fiber length $l_f$. It can be seen that the theoretical expression produces reasonably accurate predictions across the complete range of crack spacing values, with the exception of a test by Leutbecher and Fehling [24].

With the predicted crack spacing, Eq. (3) can be used to predict the complete tension force vs. average tensile strain response of reinforced UHPFRC members. This equation is applied to a test specimen from Jungwirth and Muttoni [23]. The specimen had a cross section of 160x160 mm, and was reinforced with 4ϕ16 rebars and 2.5% of steel fibers with $l_f = 20$ mm and $d_f = 0.3$ mm. The yield strength of the reinforcement was $f_y = 556$ MPa; the compressive strength of the UHPFRC was $f_c' = 190$ MPa; and the tensile strength was $f_{ct} = 8.8$ MPa.

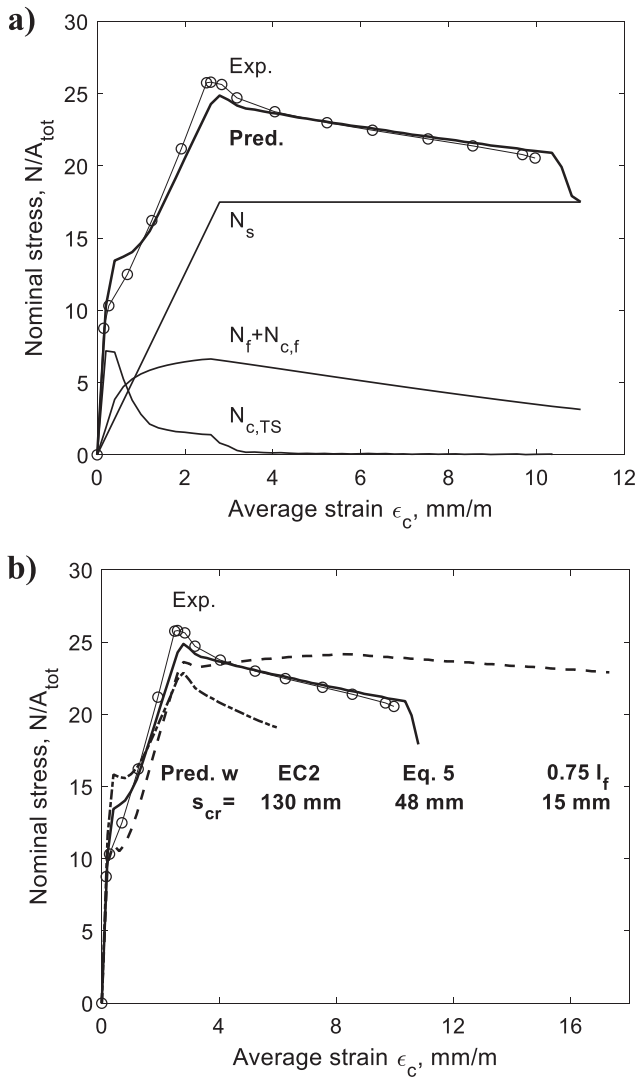


**Fig. 4.** Measured vs. predicted response of a reinforced UHPFRC member subjected to uniaxial tension (prediction generated with program VecTor2 [28,29]) – test 2.5% by Jungwirth and Muttoni [23]. (a) Prediction with crack spacing from Eq. 5, (b) Effect of crack spacing.

In Fig. 4a, the measured $N$-$\varepsilon_c$ response of this specimen is compared to the prediction from Eq. (3)—generated using an input crack spacing of 48 mm obtained from Eq. (5). The plot demonstrates that the model captures the entire range of the measured response, including the peak resistance and the post-peak behavior. The figure also shows the different components of Eq. (3) and how they vary with increasing strain. According to these components, the fibers contributed 26% to the peak resistance of the member.

Fig. 4b uses the same specimen to study the effect of crack spacing on the predicted $N$-$\varepsilon_c$ response. In addition to the crack spacing predicted by Eq. (5), two other spacing values are used—15 mm and 130 mm. The smaller value is equal to $0.75l_f$ [23] and corresponds to a hardening UHPFRC, while the larger one is obtained from the EC2 equation (Eq. 7.11) for reinforced concrete without fibers[27]. Fig. 4b demonstrates that the crack spacing plays a major role for the accurate prediction of the post-peak response, yet does not have a significant effect on the peak resistance. A crack spacing of 15 mm results in a significant overestimation of the ductility of the member, while a spacing of 130 mm results in an underestimated ductility. It should be noted that the accurate prediction of the post-peak behavior is crucial for the modeling of shear-critical UHPFRC members, where a significant redistribution of stresses can occur in the web following the yielding of the stirrups.

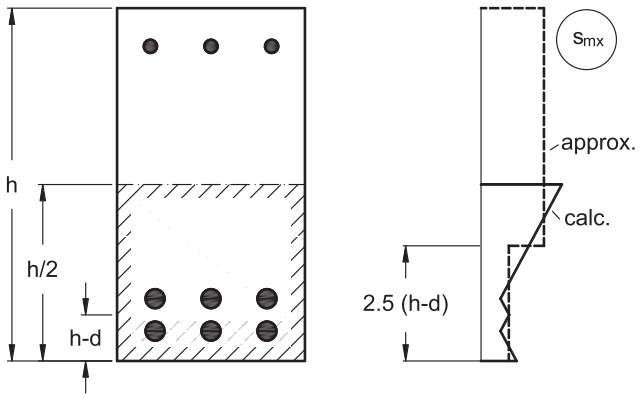


**Fig. 5.** Variation of the horizontal crack spacing along the depth of beams.

### 2.3. Crack spacing in the webs of UHPFRC beams

The crack spacing evaluated from Eq. (5) is valid for the cracks that develop in the vicinity of (and perpendicular to) rebars. In the web of UHPFRC beams, however, the cracks are inclined due to shear effects and develop away from the main flexural rebars. To capture this phenomenon, the proposed modeling approach employs a more general equation which calculates the spacing between inclined cracks as a combination of two constituents, as follows [28]:

$$s_{cr} = \frac{1}{\frac{\cos^2\theta}{s_{mx}} + \frac{\sin^2\theta}{s_{my}}} \tag{10}$$

where $s_{mx}$ and $s_{my}$ are the spacing between the vertical and horizontal cracks, respectively; and $\theta$ is the angle of the inclined cracks with respect to the axis of the beam. Therefore, to evaluate $s_{cr}$, it is necessary to evaluate separately $s_{mx}$ and $s_{my}$—as if the member is subjected separately to tension parallel to the longitudinal and transverse reinforcement, respectively.

The evaluation of the horizontal crack spacing $s_{mx}$ is illustrated in Fig. 5. At the level of the bottom flexural reinforcement, the spacing is minimum and increases linearly away from the reinforcement. This formulation is adopted from Collins and Mitchell [30] who applied it to reinforced and prestressed concrete beams based on an earlier crack spacing expression [31]. Using the same approach, Eq. (5) for UHPFRC is extended to:

$$s_{mx} = \max\left[\frac{\left(\sigma^i_{cf,cr} - \sigma_{cf0}\right)d_s}{2\tau_{sm}\rho_s}, 0.75l_f\right] + Kc_x \tag{11}$$

where $d_s$ is the diameter of the longitudinal reinforcement with a total area of $A_s$; $\rho_s = A_s/A_{cb}$ is the reinforcement ratio calculated for the area of the concrete $A_{cb}$ in the bottom one-half of the section; $c_x$ is the distance from the reinforcement to the location where the crack spacing is evaluated, and factor $K$ controls how fast the crack spacing increases away from the reinforcing bars. Assuming also that $\sigma^i_{cf,cr}/(2\tau_{sm}) \approx f_{ct}/(2\tau_{sm}) \approx 0.15$, the expression for the spacing of the vertical cracks is simplified to:

$$s_{mx} = \max\left[\left(0.15 - \frac{0.2\alpha_f V_f l_f}{d_f}\right)\frac{d_s}{\rho_s}, 0.75l_f\right] + Kc_x \tag{12}$$

For concrete members without fibers, coefficient $K$ is estimated at 2 [30]. For UHPFRC exhibiting hardening behavior, $K$ should be taken as zero, since the reinforcement is not needed to control the cracks. Consequently, the proposed modeling approach varies $K$ linearly from 2 to zero as the volume of fibers $V_f$ increases from zero to $V_{f,\max}$:

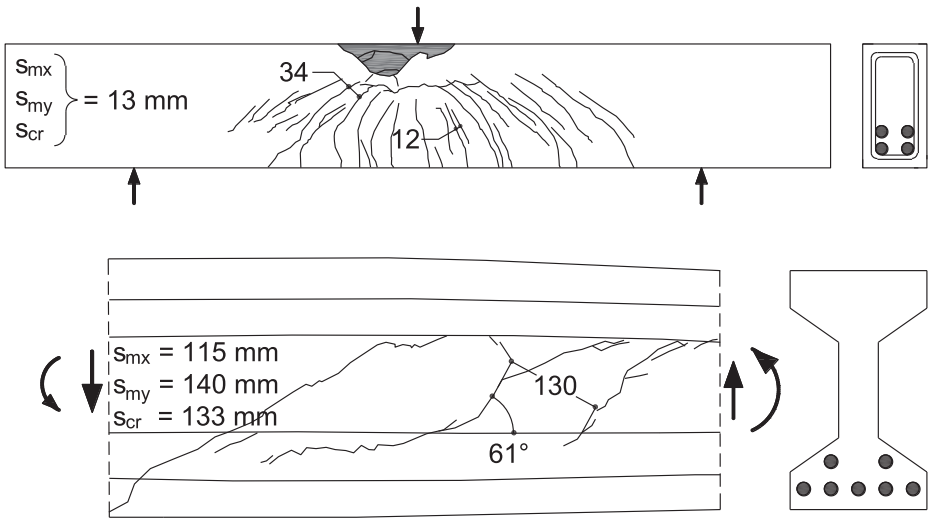


**Fig. 6.** Measured and predicted spacing of the inclined cracks in the web of reinforced UHPFRC beams – specimens SB2 [32] (top) and B29 [33] (bottom).

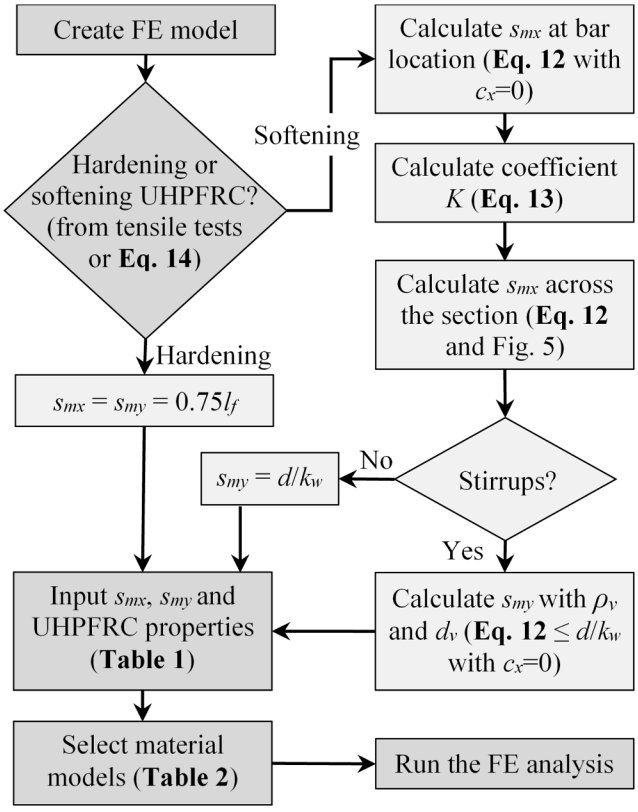


**Fig. 7.** Modeling methodology.

$$K = 2\left(1 - \frac{V_f}{V_{f,max}}\right) \geq 0 \tag{13}$$

where $V_{f,\max}$ is the ratio separating a hardening from a softening UHPFRC. This ratio is estimated by setting the expression inside the round brackets in Eq. (12) equal to zero:

$$V_{f,\max} = 0.75 \frac{d_f}{\alpha_f \cdot l_f} \tag{14}$$

As indicated with the dashed lines in Fig. 5, the calculated linear variation of the crack spacing $s_{mx}$ across the section in Eq. (12) can be simplified as a stepwise function. For finite element modeling, it is convenient to use only two $s_{mx}$ values: one in the vicinity of the flexural reinforcement and the other in the rest of the section. The former value is obtained by averaging the linearly-varying crack spacing within an effective tension zone with a depth of $\min[2.5(h - d), h/2]$ [27] at the bottom of the section. The latter value is calculated by averaging the crack spacing in the rest of the bottom one-half of the section. In I-sections, the depth of the effective tension zone can be taken as the thickness of the tension flange.

As a last step, the vertical crack spacing $s_{my}$ should be evaluated as required by Eq. (10). For beams without stirrups, $s_{my}$ depends entirely on

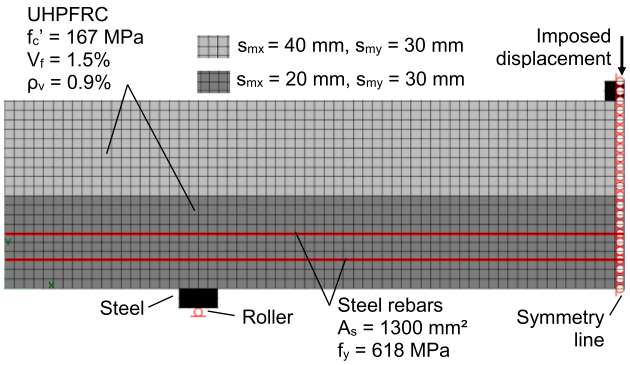


**Fig. 8.** A typical finite element model of a beam test specimen under symmetrical three-point bending.

**Table 2**
Material models in program VecTor2.

| Material behavior to be modeled | Recommended model for UHPFRC |
|---|---|
| Compression pre-peak | Lee et al. 2011 (FRC) [19,36] |
| Compression post-peak | Lee et al. 2011 (FRC) [19,36] |
| Tension softening | Exponential [28] |
| Crack width check | Omitted* |
| Cracking spacing | User input |

* intended for reinforced concrete members.

the tension behavior of the UHPFRC. If the material exhibits a hardening behavior (i.e., $V_f \geq V_{f,\max}$), the crack spacing is calculated as $0.75l_f$, and if the material is softening ($V_f < V_{f,\max}$), $s_{my}$ is estimated as $d/k_w$. When used in Eq. (4) for evaluating crack widths, this latter value corresponds to a single horizontal crack within the depth of the member. If the section has flanges, the effective depth $d$ can be replaced by the clear depth of the web between the flanges. For beams with stirrups, $s_{my}$ is obtained from Eq. (12), where $d_s$ is replaced by the stirrup diameter $d_v$; $\rho_s$ is replaced by the stirrup ratio $\rho_v$; and $K$ is set to zero. In any case, the calculated crack spacing should not be taken larger than that found in beams without stirrups (i.e., $s_{cr} \leq d/k_w$).

This formulation for the spacing of the inclined web cracks in reinforced UHPFRC beams is validated with tests from the literature. Fig. 6 shows the crack diagrams obtained from two tests performed by Lim and Hong [32] and Randl [33]. Specimen SB2 in the figure had a rectangular section with hardening UHPFRC, while specimen B29 featured an I-section with softening UHPFRC. The stirrup ratios of the two beams were respectively 0.6% and 0; and the fiber volume ratios were 1.5% and 1%. The details of the specimens are provided in Table A1 in the appendix. The crack spacing $s_{cr}$ is evaluated using Eq. (10), where $s_{mx}$ and $s_{my}$ are calculated as discussed above, while angle $\theta$ is estimated from the crack diagrams. As shown in Fig. 6, the predicted average crack spacing of 13 mm for specimen SB2 fits in the range of measured values varying from ~12 mm to ~35 mm. For B29, the predicted and measured values are 133 mm and ~130 mm, respectively. It should be noted however that the crack propagation in webs is a very complex phenomenon, and the predictions of the proposed equations should only be seen as estimates.

## 3. Application of the proposed modeling approach

The proposed modeling approach employs the formulations described above within the framework of the Disturbed Stress Field Model (DSFM) [34]. The DSFM is a smeared, rotating crack model that originates from the Modified Compression Field Theory for reinforced concrete elements subjected to shear [35]. The formulation described by Eq. (3) is used in the DSFM to model the tension behavior perpendicular to the cracks. The fibers are also taken into account in the compression

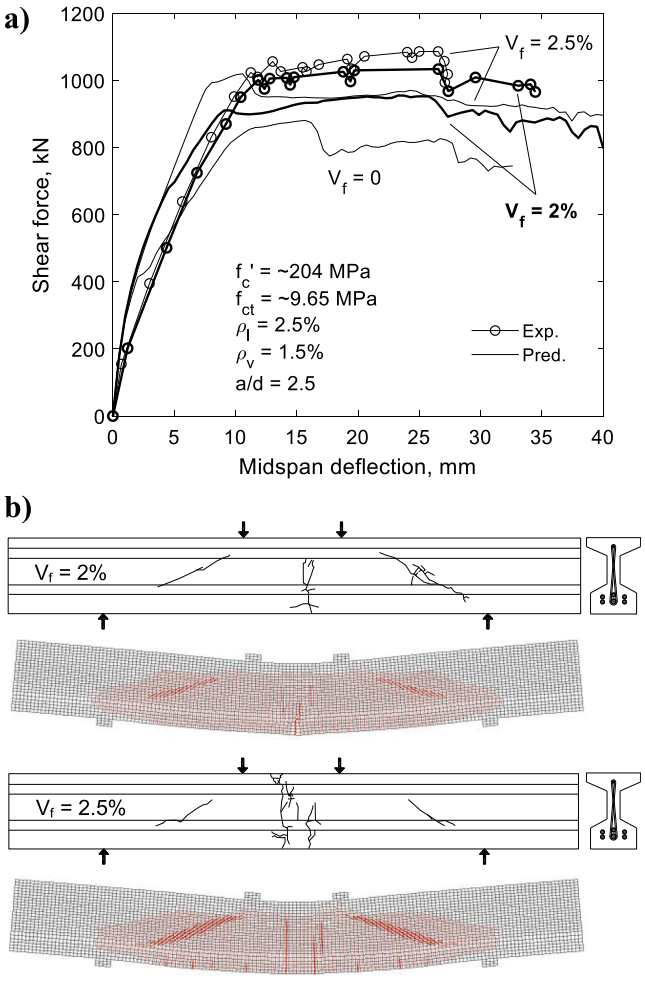


**Fig. 9.** Measured and predicted response of flexure-critical beams – specimens 4A and 4B [37]. (a) Global response, (b) Crack patterns at failure.

response of the concrete parallel to the cracks, as well as in calculating the slip displacements in the cracks. The DSFM and the material models employed by the proposed modeling approach are already implemented into the computer program VecTor2 [28,29]. While this study uses VecTor2 for nonlinear finite element modeling purposes, the proposed modeling approach can also be employed through the use of other computational modeling platforms. The main steps of the modeling approach are outlined in the flowchart in Fig. 7.

The first step is to create a finite element model including the mesh and boundary conditions; see the beam in Fig. 8 as an example. The concrete is modelled with 15 to 20 2D quadrilateral elements across the depth of the section, while the bottom and top longitudinal reinforcement is modelled with discrete 1D truss elements with a perfect bond. The stirrups (if present) are either smeared into the concrete elements as vertical steel components, or modelled as discrete truss bars if the spacing is not constant throughout.

The next step is to characterize the UHPFRC used in the member as either strain-softening or -hardening. This decision should ideally be made based on the results from tensile material tests. In the absence of such tests, the UHPFRC can be considered as softening when the fiber volume ratio $V_f$ does not exceed $V_{f,\max}$ as formulated in Eq. (14). As evident from the flowchart, this characterization is essential for the determination of the crack spacing. In hardening UHPFRC, $s_{mx}$ and $s_{my}$ are taken as $0.75l_f$, while a more detailed procedure is employed for the softening UHPFRC. This procedure accounts for the effects of the longitudinal, transverse, and fiber reinforcement on the spacing of normal and inclined cracks. The crack spacings $s_{mx}$ and $s_{my}$ are calculated for

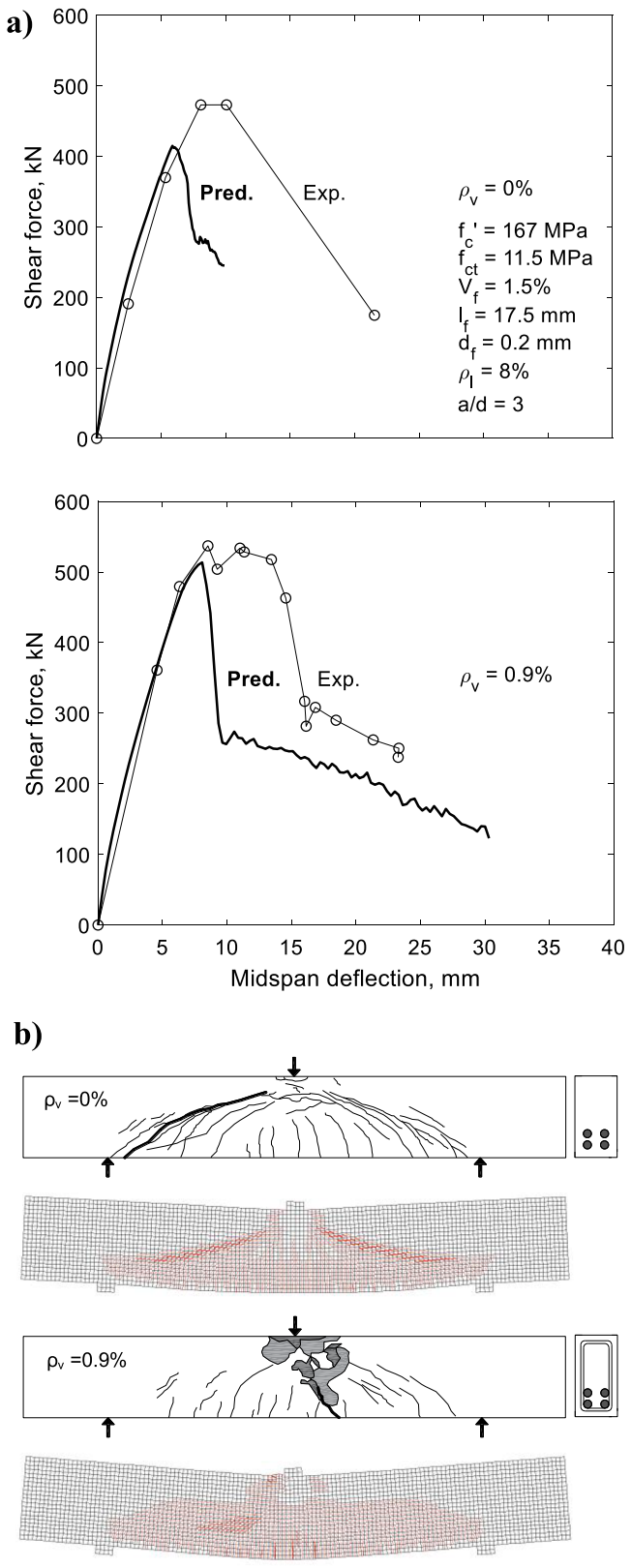


**Fig. 10.** Measured and predicted response of shear-critical beams – specimens SB1 and SB3 by Lim and Hong [32]. (a) Global response. (b) Crack patterns at failure.

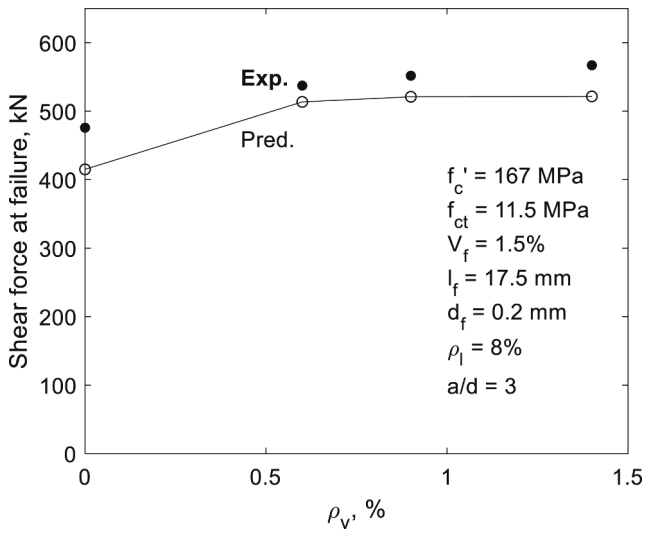


**Fig. 11.** Effect of stirrup ratio – specimens SB1 to SB4 by Lim and Hong [32].

two zones, as shown in Figs. 5 and 8, with one zone located in the vicinity of the flexural tension reinforcement and the other zone in the web above the reinforcement. In addition to the crack spacings, the modeling approach also requires a number of other input material properties, as summarized in Table 1. As indicated in the table, it is preferred to use experimentally-determined input values when available. Note however that, apart from the tensile strength $f_{ct}$, these values do not include other points from the tension response of the UHPFRC (e.g. $\sigma_{cf0}$) as this response is predicted by the diverse embedment model. The crack orientation factor $\alpha_f$ is also evaluated based on the general approach proposed by Wong et al. [28] which takes into account the thickness of the member. In the final step, the constitutive laws are defined to describe the nonlinear behavior of concrete and reinforcement, accounting for effects such as tension softening, tension stiffening, and compression softening of the concrete. The recommended material behavior models for UHPFRC are provided in Table 2.

## 4. Experimental validation

### 4.1. Behavior of flexural-critical beams

The proposed modeling approach is first validated with 15 flexure-critical reinforced UHPFRC beams. Two representative beams (specimens 4A and 4B, tested by Baby et al. [37]) are discussed in this section as samples (see Table A1). The beams had a 380-mm-deep I-section and were subjected to symmetrical four-point bending with a shear-span-to-depth ratio $a/d = 2.5$. The flexural reinforcement ratio was 2.5% and the compressive strength of the UHPFRC was approximately 200 MPa. The beams differed only in the amount and size of the steel fibers, with a constant aspect ratio $l_f/d_f$ of 66. Specimens 4A and 4B had fibers with $l_f$ = 20 mm and 13 mm, and $V_f = 2.5\%$ and 2.0%, respectively. The main results from the calculations, including the crack spacing and the maximum tensile stress that the fibers can transfer across the cracks, are listed in Table A2.

Fig. 9**a** shows the measured and predicted load-deflection responses of the beams. As expected for flexure-critical members with high concrete strength, the beams exhibited significant flexural yielding and ductility. The increase of steel fibers from 2.0% to 2.5% resulted in a minor 5% increase in the flexural capacity. As evident from Fig. 9a, the proposed modeling approach captures this subtle difference, albeit with a slight underestimation in the peak resistances of both beams. If one of the beams was analyzed without fibers (see $V_f = 0$ line), the model would predict that 2.5% fibers result in a 16% increase in the flexural strength, which shows the significant effect of fibers on the global

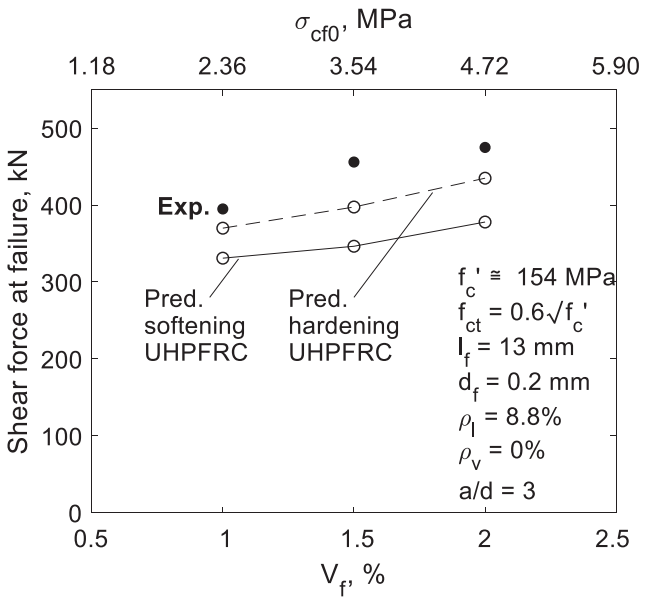


**Fig. 12.** Effect of fiber volume ratio – shear-critical specimens US2-1-3, US2-1.5-3, and US2-2-3 by Hussein and Amleh [38].

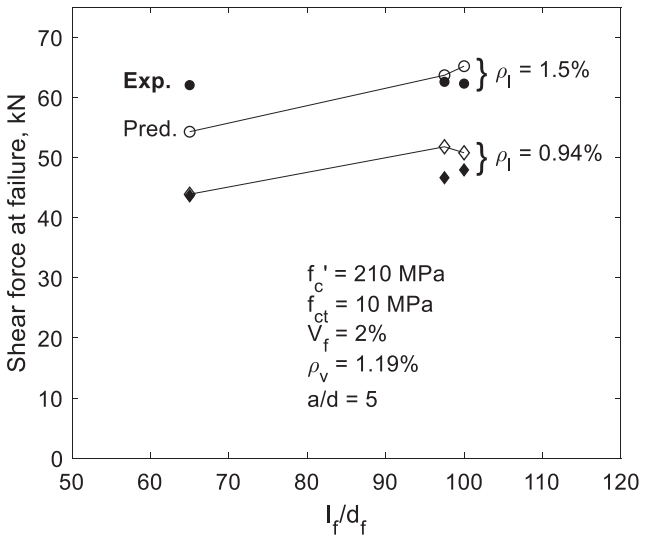


**Fig. 13.** Effect of fiber aspect ratio – flexure-critical specimens by Yoo and Yoon [41].

response of the beams.

Fig. 9b compares the measured and predicted crack diagrams of specimens 4A and 4B near failure. In addition to the critical flexural cracks in the pure-bending region, shear cracks were also observed in both shear spans. Both the flexural and shear cracks are predicted by the model. As it can be expected, the smeared crack approach resulted in more defused crack patterns than those observed in the tests.

### 4.2. Behavior of shear-critical beams

While the shear cracks in specimens 4A and 4B were not critical, it is also of interest to study reinforced-UHPFRC beams that failed in shear along inclined cracks. Such beams were tested by Lim and Hong [32] who focused on the effect of the stirrup ratio (see beams SB in Table A1). The beams had a 290 mm deep rectangular section and were tested under symmetrical three-point bending with an $a/d$ ratio of 3.0. The fiber volume ratio was 1.5% and the stirrup ratio was varied from 0 to 1.4%.

Fig. 10a shows the measured and predicted load-deflection behaviour of two of these beams: SB1 without stirrups and SB3 with $\rho_v = 0.9\%$. As expected for shear-critical members, the response of these specimens was distinctly more brittle than that of specimen 4A and 4B. As evident from Fig. 10a, the proposed modeling approach captured well the pre-peak response and underestimated the shear strength by a maximum of 15%. This most conservative strength prediction was obtained for the beam without stirrups in which the shear across the critical cracks was carried mainly by the steel fibers.

Fig. 10b compares the measured and predicted crack diagrams of specimens SB1 and SB3 near failure. It can be seen that the two experimental crack patterns differ significantly. Specimen SB1 without stirrups exhibited a typical shear failure along an inclined crack, while specimen SB3 also exhibited crushing in the vicinity of the applied load. This indicates that a stirrup ratio of 0.9% was nearly sufficient to suppress the shear failure and to force a flexural failure in the midspan region. As the beams had a very large amount of flexural reinforcement (i.e., $\rho_l = 8.0\%$), flexural failure was expected to occur with crushing of the concrete in the compression zone prior to yielding of the bottom longitudinal bars.

#### 4.2.1. Validation with experimental test series incorporating different test variables

While predicting the complete load-deflection response of reinforced UHPFRC members is important for evaluating serviceability and ductility, the most important result of the numerical simulations is the strength (i.e., load-bearing capacity or peak load capacity) of the member. Therefore, it is of interest to study how the proposed modeling approach captures the effects of various member properties on the peak load capacity.

Fig. 11 summarizes the results obtained for specimens SB1 to SB4 [32] as a function of the stirrup ratio. As $\rho_v$ is increased from 0 to 1.4%, the experimental peak load capacity increases by 19%. Most of this increase occurs up to stirrup ratios of 0.6–0.9%, followed by a nearly constant strength for larger $\rho_v$ values. This upper bound on the strength is explained by the fact that large amounts of stirrups suppress diagonal tension failure, and force a flexural failure. Indeed, specimen SB4 (with a $\rho_v$ of 1.4%) failed in flexure with crushing of the concrete in the compression zone. It is evident that the proposed modeling approach captures well the experimental trend, while being slightly conservative across the whole range of $\rho_v$ values.

In addition to providing stirrups, another way to increase the shear resistance is to increase the amount of fibers in the UHPFRC. The effect of this variable was studied by Hussein and Amleh [38,39] who tested 300-mm-deep rectangular beams with an $a/d$ ratio of 3.0 (see Table A1). The beams had no stirrups while three of them contained fibers with ratios of 1%, 1.5%, and 2% (specimens US2-1-3, US2-1.5-3, and US2-2-3). The variation of the shear force at failure of these beams with increasing $V_f$ ratio is illustrated in Fig. 12. According to the test results, as $V_f$ was doubled from 1% to 2%, the peak load capacity increased by 20%, and the specimen with 2% fibers failed in flexure. As evident from Fig. 12, the modeling approach follows the experimental trend reasonably well, but underestimates the strength of the three beams by up to 32%. These conservative predictions can be explained in part by the difficulty of predicting whether the concrete has a softening or hardening behavior. While the three UHPFRC mixes are predicted to have a softening behavior ($V_f < V_{f,\max}$ acc. to Eq. (14)), the authors of the tests used a hardening constitutive law in their numerical analyses [40]. If a hardening behavior is assumed, the results improve significantly, as illustrated by the dashed line in Fig. 12.

The results in Fig. 12 can also be analyzed from a different perspective: they illustrate the effect of the fiber pull-out resistance $\sigma_{cf0}$ and the crack spacing $s_{cr}$ on the shear strength of reinforced UHPFRC

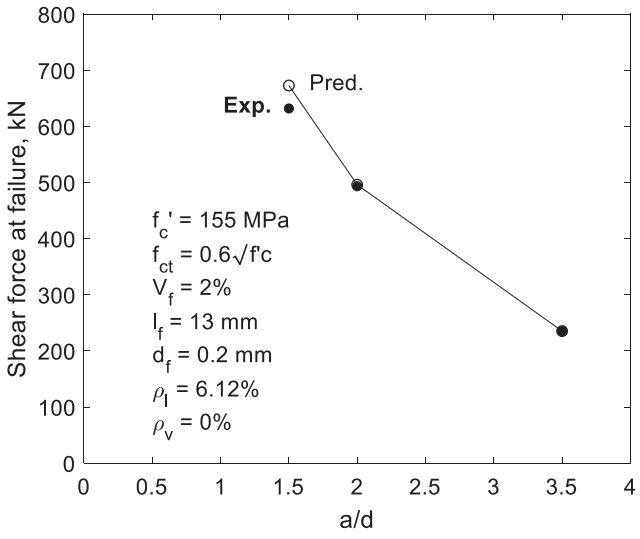


**Fig. 14.** Effect of shear-span-to-depth ratio – flexure-critical specimens US1-2-1.5/US1-2-2/US1-2-3.5 by Hussein and Amleh [38].

members. As pull-out resistance is proportional to $V_f$ according to the SDEM and Eq. (8), the curves in the plot also show the $\sigma_{cf0}$ vs. shear strength trend (see the top horizontal axis), where $\sigma_{cf0}$ is predicted to vary from 2.36 MPa to 4.72 MPa (SDEM values). The effect of the crack spacing, on the other hand, is reflected in the difference between the "softening UHPFRC" and "hardening UHPFRC" prediction curves. Indeed, when the input is changed from softening to hardening material, the only modification is the crack spacing. For a softening UHPFRC, the spacing between vertical cracks in the web is predicted at (68-46-25) mm, and that between the horizontal cracks at (35-27-22) mm. When a hardening UHPFRC is considered, both spacings are reduced to $0.75l_f =$ 9.75 mm. Larger $\sigma_{cf0}$ means larger stresses along the critical shear crack at failure, and smaller crack spacing means more uniform stresses along the crack. Therefore, $\sigma_{cf0}$ and smaller $s_{cr}$ result in an increased shear resistance of reinforced UHPFRC beams. The values of fiber pull-out resistance and crack spacing for all members modeled in this study are listed in the Appendix, Table A2.

The results in Fig. 12 can also be analyzed from a different perspective: they illustrate the effect of the fiber pull-out resistance $\sigma_{cf0}$ and crack spacing $s_{cr}$ on the shear strength of reinforced UHPFRC members. As the pull-out resistance is proportional to the volume of fibers (Eq. (8)), the $V_f$ values on the horizontal axis can be replaced with

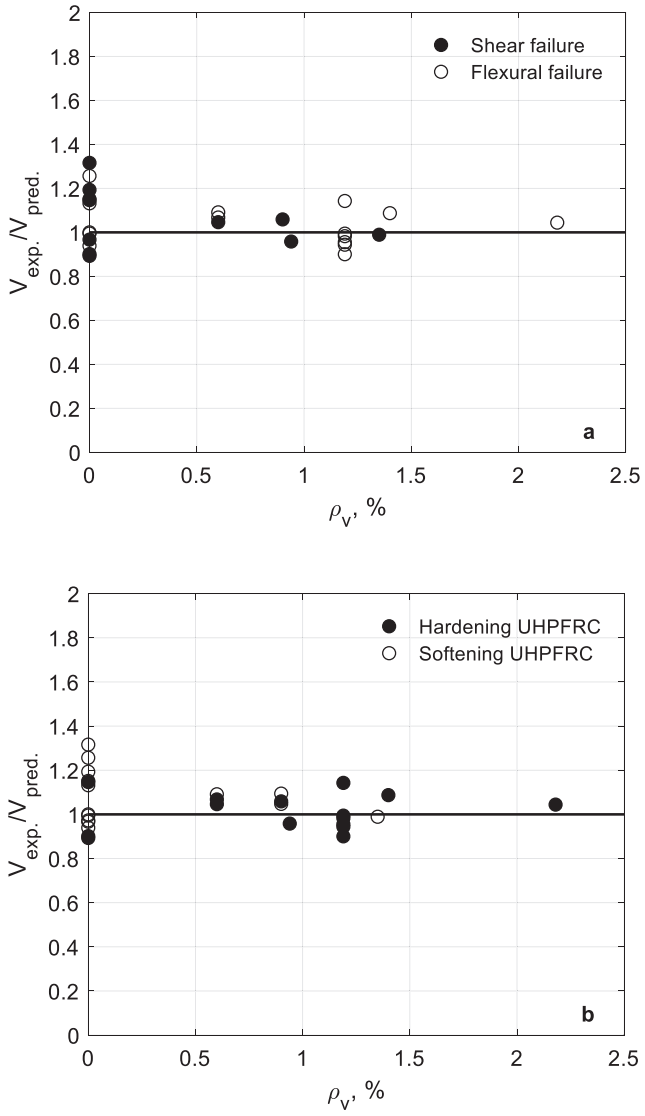


**Fig. 15.** Experimental-to-predicted strength ratios for a database of 29 reinforced UHPFRC tests.

the corresponding $\sigma_{cf0}$ values varying from 3 MPa ($V_f = 1\%$) to 6 MPa ($V_f = 2\%$). The effect of the crack spacing, on the other hand, is reflected in the difference between the "softening UHPFRC" and "hardening UHPFRC" prediction curves. Indeed, when the input of the model is changed from a softening to hardening material, the crack spacing is reduced to $0.75l_f$, and this results in a more ductile tensile behavior of the UHPFRC. The larger is $\sigma_{cf0}$, the larger are the tensile stresses along the critical shear crack at failure. The smaller is the crack spacing, the more uniform are the tensile stresses along the crack. Therefore, larger $\sigma_{cf0}$ and smaller $s_{cr}$ result in an increased shear resistance of reinforced UHPFRC beams as illustrated in Fig. 12.

Another variable related to the steel fibers is the aspect ratio $l_f/d_f$, which was studied through six beam tests reported by Yoo and Yoon [41]. The beams had a 210-mm-deep rectangular section with an $a/d$ ratio of 5, and all failed in flexure (see Table A1). The $l_f/d_f$ ratio was varied from 65 to 100 by varying both the length and the diameter of the fibers, while the fiber volume ratio was kept constant at 2%. As evident from Fig. 13, the measured flexural strengths of the specimens with $\rho_l = 1.5\%$ was almost unaffected by the $l_f/d_f$ ratio, while those of the beams with $\rho_l = 0.94\%$ increased by 10% as $l_f/d_f$ increased from 65 to 100. As demonstrated in the plot, the proposed modeling approach produces adequate strength predictions with the exception of specimen S13H, whose peak load capacity has been underestimated.

The last variable studied is the shear-span-to-depth ratio, as presented in Fig. 14. The beams used in this study had a 300-mm-deep rectangular section and variable shear spans resulting in $a/d$ ratios of 1.5, 2.0, and 3.5 (specimens US1-2-1.5, US1-2-2, and US1-2-3.5 in Table A1) [38]. All three specimens failed in flexure in the experiments. Since their sectional and material properties were nominally identical, the trend in Fig. 14 is inversely proportional to the shear span $a$ of the beams. As evident from the figure, the proposed modeling approach produces excellent predictions of the flexural strength of the beams.

### 4.3. Summary of test results and predictions

Fig. 15 presents the experimental-to-predicted strength ratios of the reinforced UHPFRC beams—plotted as a function of the stirrup ratio for all 29 test specimens modelled in this study (see Table A1). Fig. 15a compares the results for flexure- and shear-critical specimens, while Fig. 15b compares softening and hardening UHPFRC. As evident from Fig. 15a, the proposed modeling methodology produces excellent predictions for all flexure-critical members and for the shear-critical beams with transverse reinforcement (i.e., stirrups). As can be expected, the scatter in the predictions is larger for beams without stirrups, due to the challenges associated with modeling the inherent randomness in their brittle failures. Within this group with $\rho_v = 0$, Fig. 15b shows that the proposed approach accurately captures the strengths of the beams with hardening UHPFRC. Only a few tests of softening UHPFRC specimens with $\rho_v = 0$ are predicted with larger conservatism (max $V_{exp}/V_{pred}$ ratio of 1.32). These ratios are well within the error margins one could expect from the nonlinear analysis of UHPFRC, considering that the proposed modeling approach has a general applicability to many material mixes and member configurations (see Table A1), and that a similar or even larger scatter could also be obtained for regular reinforced concrete beams with $\rho_v = 0$ [42]. Considering all 29 specimens, the proposed modeling approach provided adequate accuracy, with an average of 1.04 and a coefficient of variation (COV) of 10.2% for the experimental-to-predicted strength values.

## 5. Conclusions

This paper presented a numerical modeling approach for reinforced UHPFRC members by extending the Simplified Diverse Embedment Model, which was originally developed for regular-strength fiber reinforced concrete. A set of comprehensive crack spacing formulations were established, and a new bond resistance limit was proposed. The proposed modeling approach was employed within the framework of a smeared, rotating crack model based on the Disturbed Stress Field Model. The proposed approach was validated with 29 large-scale specimens reported by seven different research groups. The simulated load vs. deflection responses, crack patterns, and failure modes were examined in detail and compared with the experimental data. Essential modeling recommendations were made to accurately capture the unique behavior of UHPFRC using nonlinear finite element models. The main contributions and findings of the study are the following:

1. Simple relationships are proposed to estimate the important properties of UHPFRC, including the tensile strength of the matrix and softening or hardening behavior—entirely based on the readily-available input quantities such as the compressive strength of the concrete, the fiber length, and fiber diameter.
2. A new increased bond stress limit is proposed for modeling UHPFRC based on test data available in the literature. The simulation results have demonstrated the suitability of this limit for modeling beams made from both hardening and softening UHPFRC.
3. It was found that the predictions are very sensitive to the crack spacing, which is a common input parameter in numerical models. The crack spacing is used to transform average tensile strains into crack widths—necessary for the evaluation of the stresses transferred by the fibers in the cracks.
4. For reinforced UHPFRC members subjected to axial tension, the crack spacing is evaluated based on a set of formulations considering the equilibrium of the concrete between the cracks. This approach has produced reasonably accurate estimates of the maximum crack spacing measured in tests, as well as adequate predictions of the pre- and post-peak behaviors of test specimens in tension.
5. For reinforced UHPFRC beams, it has been found that it is crucial to accurately evaluate the spacing of the inclined web cracks, taking into account the effect of flexural reinforcement, stirrups, and fibers. These factors have been included in the proposed formulations, which are shown to produce reasonably accurate predictions of the crack spacing measured in test specimens with both strain-softening and -hardening UHPFRC.
6. The predicted crack spacings were used within the proposed modeling approach to simulate the complete behavior of 15 flexure-critical and 14 shear-critical beams—made from either hardening or softening UHPFRC with either I-shaped or rectangular cross sections. The simulation results demonstrate that the model captures the pre-peak and peak responses very well, while remaining on the conservative side for the displacement capacities of shear-critical beams.
7. For all 29 beams modelled in this study, the proposed modeling approach produced an average experimental-to-predicted strength ratio of 1.04 with a coefficient of variation of 10.2%. The results are on the conservative side for shear-critical specimens without shear reinforcement and with strain-softening UHPFRC.

## Declaration of Competing Interest

The authors declare that they have no known competing financial interests or personal relationships that could have appeared to influence the work reported in this paper.

## Appendix A

See Tables A1 and A2.

**Table A1**
Summary of 29 reinforced UHPFRC beam tests.

| Ref. | Specimen | $b_w$ (mm) | $b_{f,top}$ (mm) | h (mm) | d (mm) | a/d | $f_c$' (MPa) | $E_c$ (GPa) | $f_{ct}$ (MPa) | $V_f$ (%) | $l_f$ (mm) | $d_f$ (mm) | $\rho_v$ (%) | $f_{yv}$ (MPa) | $\rho_l$ (%) | $f_y$ (MPa) | $V_{exp}$ (kN) | $V_{exp}/V_{pred}$ | UHPFRC type | Mode of failure | Section type |
|---|---|---|---|---|---|---|---|---|---|---|---|---|---|---|---|---|---|---|---|---|---|
| [43] | – | 20 | 200 | 200 | 180 | 2.8 | 150 | 47 | 10 | 3 | 13 | 0.16 | 0.94 | *500* | 2.18 | 500 | 230 | 0.96 | H | S | I |
| | – | 20 | 200 | 200 | 180 | 2.8 | 150 | 47 | 10 | 3 | 13 | 0.16 | 0 | – | 2.18 | 500 | 184 | 0.89 | H | S | I |
| [33] | B15-26* | 58 | 200 | 350 | 320 | 3.5 | 166.25 | *50* | *7.73* | 2 | 15 | 0.2 | 1.35 | 550 | 3.44 | 900 | 757 | 0.99 | *S* | S | I |
| | B17 | 58 | 200 | 350 | 320 | 3.5 | 170.4 | *50* | *7.82* | 2 | 15 | 0.2 | 0.9 | 550 | 3.44 | 900 | 704 | 1.05 | *S* | S | I |
| | B19-25–30* | 58 | 200 | 350 | 320 | 3.5 | 174.4 | *50* | *7.95* | 2 | 15 | 0.2 | 0 | – | 3.44 | 900 | 488 | 0.97 | *S* | S | I |
| | B28 | 58 | 200 | 350 | 320 | 3.5 | 165.8 | *50* | *7.73* | 1 | 15 | 0.2 | 0.9 | 550 | 3.44 | 900 | 628 | 1.09 | *S* | S | I |
| | B20-24–29* | 58 | 200 | 350 | 320 | 3.5 | 174.4 | *50* | *7.92* | 1 | 15 | 0.2 | 0 | – | 3.44 | 900 | 408 | 1.15 | *S* | S | I |
| [37] | 3A | 65 | 270 | 380 | 305 | 2.5 | 195 | 61 | 9.5 | 2.5 | 20 | 0.3 | 0 | – | 2.50 | 551 | 923 | 0.90 | H | S | I |
| | 3B | 65 | 270 | 380 | 305 | 2.5 | 212 | 56 | 9.8 | 2 | 13 | 0.2 | 0 | – | 2.50 | 551 | 910 | 0.97 | S | S | I |
| | 4A | 65 | 270 | 380 | 305 | 2.5 | 195 | 61 | 9.5 | 2.5 | 20 | 0.3 | 0.6 | 600 | 2.50 | 551 | 1089 | 1.07 | H | F | I |
| | 4B | 65 | 270 | 380 | 305 | 2.5 | 212 | 56 | 9.8 | 2 | 13 | 0.2 | 0.6 | 600 | 2.50 | 551 | 1042 | 1.09 | S | F | I |
| [38,39] | US1-1–35 | 150 | 150 | 300 | 218 | 3.5 | 153 | 47 | *7.42* | 1 | 13 | 0.2 | 0 | – | 6.12 | 474 | 660 | 1.13 | *S* | F | R |
| | US1-2–35 | 150 | 150 | 300 | 218 | 3.5 | 159 | 47 | *7.57* | 2 | 13 | 0.2 | 0 | – | 6.12 | 474 | 724 | 1.00 | *S* | F | R |
| | US1-2–2 | 150 | 150 | 300 | 218 | 2.0 | 155.5 | 47 | *7.48* | 2 | 13 | 0.2 | 0 | – | 6.12 | 474 | 750 | 0.99 | *S* | F | R |
| | US1-2–15 | 150 | 150 | 300 | 218 | 1.5 | 152 | 47 | *7.40* | 2 | 13 | 0.2 | 0 | – | 6.12 | 474 | 850 | 0.94 | *S* | F | R |
| | US2-1–3 | 150 | 150 | 300 | 213 | 3.0 | 153 | 47 | *7.42* | 1 | 13 | 0.2 | 0 | – | 8.76 | 468 | 790 | 1.19 | *S* | S | R |
| | US2-1.5–3 | 150 | 150 | 300 | 213 | 3.0 | 154 | 47 | *7.45* | 1.5 | 13 | 0.2 | 0 | – | 8.76 | 468 | 912 | 1.32 | *S* | S | R |
| | US2-2–3 | 150 | 150 | 300 | 213 | 3.0 | 154 | 47 | *7.45* | 2 | 13 | 0.2 | 0 | – | 8.76 | 468 | 950 | 1.26 | *S* | F | R |
| [41] | S13H | 150 | 150 | 220 | 177 | 5.1 | 212 | 47 | 10 | 2 | 13 | 0.2 | 1.19 | 491 | 1.50 | 510 | 124.1 | 1.14 | H | F | R |
| | S13L | 150 | 150 | 220 | 179 | 5.0 | 212 | 47 | 10 | 2 | 13 | 0.2 | 1.19 | 491 | 0.94 | 495 | 87.3 | 0.99 | H | F | R |
| | 195H | 150 | 150 | 220 | 177 | 5.1 | 210 | 47 | 10 | 2 | 19.5 | 0.2 | 1.19 | 491 | 1.50 | 510 | 125.2 | 0.98 | H | F | R |
| | 195L | 150 | 150 | 220 | 179 | 5.0 | 210 | 47 | 10 | 2 | 19.5 | 0.2 | 1.19 | 491 | 0.94 | 495 | 93.3 | 0.90 | H | F | R |
| | S30H | 150 | 150 | 220 | 177 | 5.1 | 210 | 47 | 10 | 2 | 30 | 0.3 | 1.19 | 491 | 1.50 | 510 | 124.6 | 0.96 | H | F | R |
| | S30L | 150 | 150 | 220 | 179 | 5.0 | 210 | 47 | 10 | 2 | 30 | 0.3 | 1.19 | 491 | 0.94 | 495 | 94.9 | 0.94 | H | F | R |
| [44] | UHP-FRC | 229 | 229 | 406 | 305 | 4.75 | 145 | 40 | *7.22* | 3 | 12.5 | 0.175 | 2.18 | *400* | 12.34 | *420* | 1415 | 1.04 | H | F | R |
| [32] | SB1 | 150 | 150 | 290 | 220 | 3 | 167 | 41 | 11.5 | 1.5 | 17.5 | 0.2 | 0 | 538 | 8.00 | 618 | 952 | 1.15 | H | S | R |
| | SB2 | 150 | 150 | 290 | 220 | 3 | 167 | 41 | 11.5 | 1.5 | 17.5 | 0.2 | 0.6 | 538 | 8.00 | 618 | 1075 | 1.05 | H | S | R |
| | SB3 | 150 | 150 | 290 | 220 | 3 | 167 | 41 | 11.5 | 1.5 | 17.5 | 0.2 | 0.9 | 538 | 8.00 | 618 | 1103 | 1.06 | H | S | R |
| | SB4 | 150 | 150 | 290 | 220 | 3 | 167 | 41 | 11.5 | 1.5 | 17.5 | 0.2 | 1.4 | 538 | 8.00 | 618 | 1134 | 1.09 | H | F | R |
| | | | | | | | | | | | | | | | | | **Avg.=** | **1.04** | | | |
| | | | | | | | | | | | | | | | | | **COV=** | **10.2%** | | | |

Notation: $b_w$ = width of web; $b_{f,top}$ = width of compression flange; $h$ = section depth; $d$ = effective depth of section; $a/d$ = shear-span-to-effective-depth ratio; $f_c'$ = compressive cylinder strength; $E_c$ = elastic modulus; $f_{ct}$ = tensile strength; $V_f$ = volume of fibers; $l_f$ = length of fibers; $d_f$ = diameter of fibers; $\rho_v$ = stirrups ratio; $f_{yv}$ = yield stress of stirrups; $\rho_l = A_s/b_{f,top}d$ = longitudinal reinforcement ratio where $A_s$ = area of tension reinforcement; $f_y$ = yield stress of long. reinf.; $V_{exp}$ = measured shear force at failure; $V_{pred}$ = predicted shear force at failure; UHPFRC type= "H" for strain hardening and "S" for softening; Mode of failure (reported)= "S" for shear and "F" for flexural failure; Section type= "I" for I-section and "R" for rectangular section.

Notes:

1) *Two or three nominally identical specimens with averaged $f_c$' and $V_{exp}$.

2) The italic numbers represent estimated values as measured values were not provided by the authors of the tests.

**Table A2**
Summary of main calculation results for 29 reinforced UHPFRC beam tests.

| Ref. | Specimen | d (mm) | $V_f$ (%) | $l_f$ (mm) | $d_f$ (mm) | $V_{f,max}$ (%) | UHPFRC type | $A_s$ ($mm^2$) | $\rho_s$ (%) | $d_s$ (mm) | $\rho_v$ (%) | K | $s_{mx,1}$ (mm) | $s_{mx,2}$ (mm) | $s_{my}$ (mm) | $\sigma_{cf0}$ (MPa) | $V_{pred}$ (kN) |
|---|---|---|---|---|---|---|---|---|---|---|---|---|---|---|---|---|---|
| [43] | – | 180 | 3 | 13 | 0.16 | 1.85 | H | 785 | 13.0 | 18 | 0.94 | 0 | 9.75 | 9.75 | 9.75 | 8.76 | 231 |
| | – | 180 | 3 | 13 | 0.16 | 1.85 | H | 785 | 13.0 | 18 | 0 | 0 | 9.75 | 9.75 | 9.75 | 8.76 | 202 |
| [33] | B15-26* | 320 | 2 | 15 | 0.2 | 2 | *S* | 2200 | 10.2 | 20 | 1.35 | 0 | 11.25 | 11.25 | 11.25 | 5.73 | 763 |
| | B17 | 320 | 2 | 15 | 0.2 | 2 | *S* | 2200 | 10.2 | 20 | 0.9 | 0 | 11.25 | 11.25 | 11.25 | 5.80 | 665 |
| | B19-25-30* | 320 | 2 | 15 | 0.2 | 2 | *S* | 2200 | 10.2 | 20 | 0 | 0 | 11.25 | 11.25 | 11.25 | 5.89 | 504 |
| | B28 | 320 | 1 | 15 | 0.2 | 2 | *S* | 2200 | 10.2 | 20 | 0.9 | 1.00 | 44 | 116 | 33 | 2.87 | 622 |
| | B20-24-29* | 320 | 1 | 15 | 0.2 | 2 | *S* | 2200 | 10.2 | 20 | 0 | 1.00 | 44 | 116 | 33 | 2.93 | 433 |
| [37] | 3A | 305 | 2.5 | 20 | 0.3 | 2.25 | H | 2060 | 6.2 | 22.9 | 0 | 0 | 15 | 15 | 15 | 7.06 | 1025 |
| | 3B | 305 | 2 | 13 | 0.2 | 2.3 | S | 2060 | 6.2 | 22.9 | 0 | 0.27 | 39 | 56 | 23 | 5.55 | 1026 |
| | 4A | 305 | 2.5 | 20 | 0.3 | 2.25 | H | 2060 | 6.2 | 22.9 | 0.6 | 0 | 15 | 15 | 15 | 7.06 | 1025 |
| | 4B | 305 | 2 | 13 | 0.2 | 2.3 | S | 2060 | 6.2 | 22.9 | 0.6 | 0.27 | 39 | 56 | 23 | 5.55 | 989 |
| [38,39] | US1-1-35 | 255 | 1 | 13 | 0.2 | 2.3 | *S* | 2000 | 8.9 | 25.2 | 0 | 1.13 | 72 | 107 | 35 | 2.36 | 686 |
| | US1-2-35 | 255 | 2 | 13 | 0.2 | 2.3 | *S* | 2000 | 8.9 | 25.2 | 0 | 0.27 | 28 | 36 | 22 | 4.72 | 728 |
| | US1-2-2 | 255 | 2 | 13 | 0.2 | 2.3 | *S* | 2000 | 8.9 | 25.2 | 0 | 0.27 | 28 | 36 | 22 | 4.72 | 773 |
| | US1-2-15 | 255 | 2 | 13 | 0.2 | 2.3 | *S* | 2000 | 8.9 | 25.2 | 0 | 0.27 | 28 | 36 | 22 | 4.72 | 932 |
| | US2-1-3 | 255 | 1 | 13 | 0.2 | 2.3 | *S* | 2800 | 12.4 | 29.9 | 0 | 1.13 | 68 | 96 | 35 | 2.36 | 745 |
| | US2-1.5-3 | 255 | 1.5 | 13 | 0.2 | 2.3 | *S* | 2800 | 12.4 | 29.9 | 0 | 0.70 | 46 | 63 | 27 | 3.54 | 803 |
| | US2-2-3 | 255 | 2 | 13 | 0.2 | 2.3 | *S* | 2800 | 12.4 | 29.9 | 0 | 0.27 | 25 | 31 | 22 | 4.72 | 860 |
| [41] | S13H | 177 | 2 | 13 | 0.2 | 2.3 | H | 397 | 2.4 | 15.9 | 1.19 | 0 | 9.75 | 9.75 | 9.75 | 5.54 | 115 |
| | S13L | 179 | 2 | 13 | 0.2 | 2.3 | H | 253 | 1.5 | 12.7 | 1.19 | 0 | 9.75 | 9.75 | 9.75 | 5.54 | 89 |
| | 195H | 177 | 2 | 19.5 | 0.2 | 1.5 | H | 397 | 2.4 | 15.9 | 1.19 | 0 | 15 | 15 | 15 | 8.58 | 134 |
| | 195L | 179 | 2 | 19.5 | 0.2 | 1.5 | H | 253 | 1.5 | 12.7 | 1.19 | 0 | 15 | 15 | 15 | 8.58 | 108 |
| | S30H | 177 | 2 | 30 | 0.3 | 1.5 | H | 397 | 2.4 | 15.9 | 1.19 | 0 | 22.5 | 22.5 | 22.5 | 9.04 | 138 |
| | S30L | 179 | 2 | 30 | 0.3 | 1.5 | H | 253 | 1.5 | 12.7 | 1.19 | 0 | 22.5 | 22.5 | 22.5 | 9.04 | 112 |
| [44] | UHP-FRC | 305 | 3 | 12.5 | 0.175 | 2.1 | H | 8621 | 18.6 | 34.9 | 2.18 | 0 | 9 | 9 | 9 | 7.53 | 1474 |
| [32] | SB1 | 220 | 1.5 | 17.5 | 0.2 | 1.7 | H | 2640 | 12.1 | 29 | 0 | 0 | 13 | 13 | 13 | 5.10 | 836 |
| | SB2 | 220 | 1.5 | 17.5 | 0.2 | 1.7 | H | 2640 | 12.1 | 29 | 0.6 | 0 | 13 | 13 | 13 | 5.10 | 990 |
| | SB3 | 220 | 1.5 | 17.5 | 0.2 | 1.7 | H | 2640 | 12.1 | 29 | 0.9 | 0 | 13 | 13 | 13 | 5.10 | 1023 |
| | SB4 | 220 | 1.5 | 17.5 | 0.2 | 1.7 | H | 2640 | 12.1 | 29 | 1.4 | 0 | 13 | 13 | 13 | 5.10 | 1040 |

Notation: $d$ = effective depth of section; $V_f$ = volume of fibers; $l_f$ = length of fibers; $d_f$ = diameter of fibers; $V_{f,max}$ = theoretical volume of fibers that separates softening from hardening UHPFRC (Eq. (14)); UHPFRC type= "H" for strain hardening and "S" for softening; $A_s$ = area of tension reinforcement; $\rho_s = A_s/A_{cb}$ = longitudinal reinforcement ratio used in Eq. (12); $d_s$ = diameter of longitudinal reinforcing bars; $\rho_v$ = stirrups ratio; $K$ = factor according to Eq. (13); $s_{mx,1}$ = horizontal crack spacing in the effective tension zone (Eq. (12) and Fig. 5); $s_{mx,2}$ = horizontal crack spacing in the rest of the section (Eq. (12) and Fig. 5); $s_{my}$ = vertical crack spacing; $k_w$ = factor according to Eq. (4); $\sigma_{cf0}$ = maximum crack stress that the fibers can transfer across a crack (acc. to SDEM with $\alpha_f = 0.5$); $V_{exp}$ = measured shear force at failure.
Note: The italic data represent estimated values as measured values were not provided by the authors of the tests.

## References


[1] Russel, G H, Graybeal BA. Ultra-High Performance Concrete : A state-of-the-art report for the bridge community. U.S. Department of Transportation; 2013.
[2] Bruhwiler E, Denarié E. Rehabilitation and strengthening of concrete structures using ultra-high performance fibre reinforced concrete. Struct Eng Int 2013;23:450–7.
[3] Charron JP, Denarié E, Brühwiler E. Permeability of ultra high performance fiber reinforced concretes (UHPFRC) under high stresses. Mater Struct/Materiaux et Constructions 2007;40:269–77. https://doi.org/10.1617/s11527-006-9105-0.
[4] Toutlemonde F, Resplendino J. Designing and building with UHPFRC: state-of-the-art and development. John Wiley and Sons; 2011.
[5] Möser B, Pfeifer C. Microstructure and durability of Ultra-High Performance Concrete. In: Proceedings of the second international symposium on ultra high performance concrete; 2008. p. 417–24.
[6] AFNOR (Association Francaise de normalisation). National addition to eurocode 2: Design of concrete structures: specific rules for Ultra-high Performance Fibre-reinforced Concrete (UHPFRC) - NF P 18-710. AFNOR; 2016.
[7] Baustoffe, Bemessung und Ausführung SS of A and E. Sia 2052. ultra-hochleistungs-faserbeton (uhfb). SIA Zurich: SIA; 2016.
[8] Japan Society of Civil Engineers. Recommendations for design and construction of Ultra high strength Fiber reinforced Concrete stuructures-draft. Concrete l. Japan Society of Civil Engineers; 2004.
[9] Gowripalan N, Gilbert IR. Design guidelines for ductal prestressed concrete beams. Australia: School of Civil and Environmental Engineering, The University of NSW; 2000.
[10] Chen L, Graybeal BA. Modeling structural performance of ultrahigh performance concrete I-girders. J Bridge Eng 2012;17:754–64. https://doi.org/10.1061/(ASCE)BE.1943-5592.0000305.
[11] Lampropoulos AP, Paschalis SA, Tsioulou OT, Dritsos SE. Strengthening of reinforced concrete beams using ultra high performance fibre reinforced concrete (UHPFRC). Eng Struct 2016;106:370–84. https://doi.org/10.1016/j.engstruct.2015.10.042.
[12] Sadouki H, Bruhwiler E, Zwicky D. Chillon Viaduct deck slab strengthening using reinforced UHPFRC: Numerical simulation of full-scale tests. In: Proceedings of the 4th international conference on concrete repair, rehabilitation and retrofitting, ICCRRR 2015 2015. https://doi.org/10.1201/b18972-80.
[13] Trüb M. Numerical modeling of high performance fiber reinforced cementitious composites. ETH Zurich; 2011.
[14] Guénet T, Baby F, Duhamel-Labrecque Y, Meulenyzer S, Sorelli L, Toutlemonde F, et al. Numerical modeling of UHPFRC tensile behavior by a micromechanics FEM model taking into account fiber orientation. In: 9th International conference on fracture mechanics of concrete and concrete structures FraMCoS-9 2016. https://doi.org/10.21012/fc9.010.
[15] Lee SC, Cho JY, Vecchio FJ. Simplified diverse embedment model for steel fiber-reinforced concrete elements in tension. ACI Mater J 2013;110:403–12. https://doi.org/10.14359/51685787.
[16] Lee SC, Cho JY, Vecchio FJ. Diverse Embedment Model for steel fiber-reinforced concrete in tension: model development. ACI Mater J 2011;108:516–25. https://doi.org/10.14359/51685787.
[17] Leutbecher T, Fehling E. Crack width control for combined reinforcement of rebars and fibres exemplified by Ultra-High-Performance Concrete. Fib Task Group 86 "Ultra High Performance Fibre Reinforced Concrete - UHPFRC"; 2008.
[18] Garneau J-F. Réhabilitation sismique des piles-murs de pont rectangulaires par chemisage en béton fibré à ultra-haute performance. Université de Montréal; 2015.
[19] Lee SC, Cho JY, Vecchio FJ. Analysis of steel fiber-reinforced concrete elements subjected to shear. ACI Struct J 2016;113:275–85. https://doi.org/10.14359/51688474.
[20] Deluce JR, Lee S, Vecchio FJ. Crack model for steel fiber-reinforced concrete members containing conventional reinforcement. ACI Struct J 2014;111:93–102.
[21] Leutbecher T. Rissbildung und zugtragverhalten von mit stabstahl und fasern bewehrtem Ultrahochfesten Beton (UHPC). Universität Kassel, 2007. https://doi.org/978-3-89958-374-8.
[22] Leutbecher T, Fehling E. Tensile behavior of Ultra-High-Performance concrete reinforced with reinforcing bars and fibers: Minimizing fiber content. ACI Struct J 2012;109:253–64. https://doi.org/10.14359/51683636.
[23] Jungwirth J, Muttoni A. Structural behavior of tension members in UHPC.In: Proceeding of International Symposium on UHPC; 2004. p. 533–46.
[24] Leutbecher T, Fehling E. Crack formation and tensile behaviour of UHPC reinforced with a combination of rebars and fibers. In: 2nd international symposium on ultra high performance concrete; 2008. p. 497–504.
[25] Walraven JC. High performance fiber reinforced concrete: progress in knowledge and design codes. Mater Struct/Materiaux et Constructions 2009;42:1247–60. https://doi.org/10.1617/s11527-009-9538-3.
[26] Redaelli D. Testing of reinforced high performance fibre concrete members in tension. In: Proceedings of the 6th Int PhD Symposium in Civil Engineering, vol. 9; 2006.
[27] European Committee of Standardization. Eurocode 2: Design of concrete structures: Part 1-1: General rules and rules for buildings (+AC:2010). Brussels: European Committee of Standardization; 2005.
[28] Wong PS, Vecchio FJ, Trommels H. VecTor2 and formworks user's manual; 2013.
[29] VTAG. VecTor2: Nonlinear finite element analysis software for reinforced concrete structures. VecTor Analysis Group (VTAG). Retrieved from http://vectoranalysisgroup.com/n.d.
[30] Collins MP, Mitchell D. Prestressed concrete structures. Response Publications; 1997.
[31] CEB-FIP Model Code for Concrete Structures; 1978.
[32] Lim WY, Hong SG. Shear tests for Ultra-High Performance Fiber Reinforced Concrete (UHPFRC) beams with shear reinforcement. Int J Concr Struct Mater 2016;10:177–88. https://doi.org/10.1007/s40069-016-0145-8.
[33] Randl N, Mészöli T, Harsànyi P. Shear behaviour of UHPC beams with varying degrees of fiber and shear reinforcement. In: high tech concrete: where technology and engineering meet - proceedings of the 2017 Fib symposium; 2017. https://doi.org/10.1007/978-3-319-59471-2.
[34] Vecchio FJ. Disturbed stress field model for reinforced concrete: formulation. J Struct Eng New York, NY 2000;126:1070–7. https://doi.org/10.1061/(ASCE)0733-9445(2000)126:9(1070).
[35] Vecchio FJ, Collins MP. Modified Compression-Field Theory for reinforced concrete elements subjected to shear. J Am Concr Inst 1986;83:219–31. https://doi.org/10.14359/10416.
[36] Lee SC, Oh JH, Cho JY. Compressive behavior of fiber-reinforced concrete with end-hooked steel fibers. Materials 2015;8:1442–58. https://doi.org/10.3390/ma8041442.
[37] Baby F, Marchand P, Toutlemonde F. Shear behavior of ultrahigh performance fiber-reinforced concrete beams. I: Experimental investigation. J Struct Eng (United States) 2014;140:1–10. https://doi.org/10.1061/(ASCE)ST.1943-541X.0000907.
[38] Hussein L, Amleh L. Shear behavior of UHPFRC beams without stirrups. In: Proceedings of the 10th Fib international PhD symposium in civil engineering; 2014. p. 437–42.
[39] Hussein L, Amleh L. Size effect of ultra-high performance fiber reinforced concrete composite beams in shear. Struct Concr 2018;19:141–51. https://doi.org/10.1002/suco.201700078.
[40] Hussein L, Amleh L. Structural behavior of ultra-high performance fiber reinforced concrete-normal strength concrete or high strength concrete composite members. Constr Build Mater 2015;93:1105–16. https://doi.org/10.1016/j.conbuildmat.2015.05.030.
[41] Yoo DY, Yoon YS. Structural performance of ultra-high-performance concrete beams with different steel fibers. Eng Struct 2015;102:409–23. https://doi.org/10.1016/j.engstruct.2015.08.029.
[42] Guner S, Vecchio FJ. Pushover analysis of shear-critical frames: Verification and application. ACI Struct J 2010;107:744–6.
[43] Telleen K, Noshiravani T, Galrito R, Bruhwiler E. Experimental investigation into the shear resistance of a reinforced UHPFRC web element. In: 8th Fib PhD Symposium in Kgs Lyngby, Denmark; 2010.
[44] Kaka VB, Kim J, Chao S-H. Formulating constitutive stress-strain relations for flexural design of Ultra High-Performance Fiber-Reinforced Concrete. In: First international interactive symposium on UHPC; 2016. https://doi.org/10.21838/uhpc.2016.46.